Hindawi
Mathematical Problems in Engineering
Volume 2017, Article ID 4047983, 10 pages
https://doi.org/10.1155/2017/4047983

Research Article

A Signal Processing Algorithm Based on 2D Matched Filtering for SSAR

Shouguo Yang, Yong Li, Kunhui Zhang, and Jianshe Liu

School of Electronics and Information, Northwestern Polytechnical University, Xi'an 710072, China

Correspondence should be addressed to Shouguo Yang; ysg_910@163.com

Received 16 April 2017; Revised 26 October 2017; Accepted 8 November 2017; Published 26 December 2017

Academic Editor: Yann Favennec

This study discusses a smart radar antenna scanning mode that combines features of both the sector-scan mode used for conventional radar and the line-scan mode used for synthetic aperture radar (SAR) and achieves an application of the synthetic aperture technique in the conventional sector-scan (mechanically scanned) radar, and we refer to this mode as sector-scan synthetic aperture radar (SSAR). The mathematical model is presented based on the principle of SSAR, and a signal processing algorithm is proposed based on the idea of two-dimensional (2D) matched filtering. The influences of the line-scan range and speed on the SSAR system are analyzed, and the solution to the problem that the target velocity is very high is given. The performance of the proposed algorithm is evaluated through computer simulations. The simulation results indicate that the proposed signal processing algorithm of SSAR can gather the signal energy of targets, thereby improving the ability to detect dim targets.

1. Introduction

When the radar detects the target remotely, the target is normally assumed to be a point located in a resolution cell, and the energy of the target echo is assumed to be evenly distributed in the resolution cell. The synthetic aperture technique is used to improve the resolution of a radar system by reducing the resolution cell size and concentrating the signal energy that contains information about the target. Because the energy density of the noise remains constant but the energy density of the target increases in the same resolution cell, the signal-to-noise ratio (SNR) is improved, which helps to detect a dim target. However, the majority of existing early-warning radar systems are ground-based radar (GBR). Synthetic aperture radar (SAR) requires a moving platform with a sufficiently high speed, which GBR systems lack. Supposing that a GBR system could perform a long-range fast line-scan relative to the target, this system would not meet the tactical requirements for a radar system. Therefore, it is not realistic to copy the working scene of airborne radar to that of GBR. In addition, the majority of existing early-warning radar systems use the mechanical scanning mode, which makes them lose the synthetic aperture function. Applying the synthetic aperture technique in a conventional mechanically scanned radar system remains an urgent problem.

Sector-scan synthetic aperture radar (SSAR) provides an effective approach for solving the mentioned problem above. SSAR is the improvement of ground-based sector-scan radar, which combines the advantages of the sector-scan method and the line-scan method. And the line-scan method is a beam moving transversely along the antenna surface quickly. In [1], the working mode and implementation method of SSAR are given. And it is found that when the radar is line-scanning quickly, regardless of whether the target is moving, the target has radial velocity relative to the receiving point, which is not the same as the ISAR. ISAR must wait for the plane to cross the beam transversely, so that it becomes passive. But SSAR can find target actively. It is also pointed out in [1] that SSAR can achieve wideband signals in slow-time dimension (i.e., azimuth dimension) by line-scan method, which provides the necessary conditions for compression in slow-time dimension. In this paper, we mainly study the signal processing algorithm of SSAR, so that the energy of target echo signal is obviously gathered to detect the weak point target. That is the fundamental purpose of SSAR. However, SAR and ISAR are mainly for high-resolution imaging of

target. Therefore, the purpose of SSAR is different from that of SAR and ISAR.

Because SSAR is derived from the traditional SAR approach, the SSAR signal processing procedure is developed based on the basic SAR algorithm, the range-Doppler algorithm [2], to achieve bidirectional (radial and transverse) pulse compression and to maximize the SNR. The main difficulty in signal processing lies in the range migration problem in the slow-time dimension for targets with high acceleration and a low SNR, that is, the fast- and slow-time dimension coupling problem. Existing methods for correcting range migration (caused by the maneuvering target) are generally to compensate the estimated parameters of the target [3–5]. These methods are highly effective for targets with high SNR but are ineffective for targets with low SNR. In addition, some documents have also proposed methods for targets with low SNR. For example, Chen et al. [6] proposed a method that eliminates the linear range migration caused by the target velocity using the keystone transform and increases the SNR by accumulating adjacent range profiles using the envelope-correlation algorithm [7] or the phase gradient autofocus (PGA) algorithm [8] to compensate for higher-order motion. These methods are effective when the acceleration is not particularly high and the SNR is not particularly low. However, to obtain a high transverse compression ratio, a relatively high acceleration is artificially generated by the SSAR method. In addition, dim targets have extremely low SNR. In this case, the method of Chen et al. cannot significantly increase the SNR by accumulating adjacent range profiles, and therefore, this method is limited to low-acceleration cases and is less effective for SSAR signal processing. Li et al. [9] proposed a method for correcting range migration (caused by the maneuvering target) for low-SNR targets. This method also involves parameter estimation, and a transverse correlation function is used to increase the SNR prior to the parameter estimation step. Therefore, this method applies to only cases in which the SNR is not too low. Tian et al. [10] and Dai and Zhang [11] proposed the generalized keystone transform, which can eliminate range migration caused by target motion of the second order and above (acceleration and jerk). Li et al. [12] proposed a fast algorithm to process the result of the generalized keystone transform. This algorithm performs a fast Fourier transform (FFT) in the transverse direction rather than pulse compression to eliminate range migration, and thus, this method does not increase the SNR. Wu et al. [13] and Zhu et al. [14, 15] proposed a two-dimensional (2D) matched-filter method that simultaneously performs radial and transverse compression and then estimates the target parameters. This method requires estimation of only the acceleration and is very effective.

For targets with a low SNR, it is not applicable for SSAR to use ordinary parameter estimation and compensation methods. Inspired by the idea of 2D matched filtering [13–15], the present study proposes a signal processing algorithm based on the principles of SSAR. The performance of this algorithm is verified through computer simulations, and this study lays a solid foundation for the practical application of SSAR.

2. Echo Signal Model

Zhang [16] noted that there are usually three types of radar echo models: the accurate model, the first-order approximate model, and the "stop-go" model. In the present study, the "stop-go" model is used. The "stop-go" model is also known as the "stop-and-hop" model and is obtained by further simplifying the first-order approximate model of the radar echo.

Supposing that the transmitting signal of the radar is $S(t)$, the receiving signal is $S_r(t) = kS(t - t_d)$ (k is the echo attenuation coefficient). In addition, let R_0 and v denote the range and the velocity of the target at time 0, respectively, and assume that the target is moving toward the radar system along the normal direction. Supposing that the transmitting signal is $S(t) = a(t)\exp(j2\pi f_0 t)$, the echo signal received by the radar can be expressed as follows:

$$S(t_k, t_m) = ka\left(t_k - \frac{2R(t_m)}{C}\right)\exp\left[j2\pi f_0\left(t_k - \frac{2R(t_m)}{C}\right)\right], \tag{1}$$

where t_k and t_m indicate fast-time and slow-time, respectively, f_0 represents the carrier frequency of the signal, $R(t_m)$ represents the range of the target at time t_m, and C represents the speed of light.

When we use the slow-time dimension information of the target, we assume a total of M pulse repetition intervals (PRIs). The slow-time t_m of the mth transmitting pulse is mT_r (T_r represents the PRI of the radar system). The relation between the fast-time and slow-time is as follows:

$$\begin{aligned} t_m &= mT_r, \\ t &= t_m + t_k. \end{aligned} \tag{2}$$

Zhang [16] showed that if LFM signals are used, the "stop-go" radar echo model must satisfy the following conditions to replace the accurate model:

$$\begin{aligned} v_{\max} &< \sqrt{\frac{\lambda C}{8T_a}}, \\ \left|v(t_m)\right| T_p &< \frac{C}{2B}, \\ a_{\max} &< \frac{\lambda}{4T_p T_a}, \end{aligned} \tag{3}$$

where $v_{\max}$ represents the maximum velocity of the target, $a_{\max}$ represents the maximum acceleration of the target, T_a represents the correlation time in the slow-time dimension, T_p represents the pulse width of the signal transmitted by the radar system, and λ represents the wavelength of the signal.

The "stop-go" model has a broad range of applications, and this model is almost always effective for radar systems, but it cannot be used for sonar systems [9].

3. SSAR Signal Processing Algorithm

Supposing that the transmitting signal is expressed as

$$\begin{aligned} S_T(t) &= \operatorname{rect}\left(\frac{t}{T_P}\right)\exp\left[j2\pi\left(f_0 t+\frac{1}{2}\mu t^2\right)\right] \\ &= \operatorname{rect}\left(\frac{t}{T_P}\right)\exp\left(j\pi\mu t^2\right)\exp\left(j2\pi f_0 t\right) \\ &= p(t)\exp\left(j2\pi f_0 t\right), \end{aligned} \tag{4}$$

where $p(t) = \operatorname{rect}(t/T_P)\exp(j\pi\mu t^2)$, the receiving signal can be expressed as

$$\begin{aligned} &S_r(t,t_m) \\ &= p\left(t-\frac{2R(t_m)}{C}\right)\exp\left[j2\pi f_0\left(t-\frac{2R(t_m)}{C}\right)\right]. \end{aligned} \tag{5}$$

Here, only the signal is considered, and noise is ignored. In this case, the "stop-go" model is used as the signal model. Because the amplitude of the receiving signal is a constant, normalization is performed.

After the receiving signal is mixed, (5) can be expressed as

$$S_{r,h}(t,t_m) = p\left(t-\frac{2R(t_m)}{C}\right)\exp\left[-j2\pi f_0\frac{2R(t_m)}{C}\right]. \tag{6}$$

Considering the effect of the beam width, (6) can be expressed as

$$\begin{aligned} S_{r,h}(t,t_m) &= p\left(t-\frac{2R(t_m)}{C}\right) \\ &\cdot\exp\left[-j2\pi f_0\frac{2R(t_m)}{C}\right]\operatorname{rect}\left(\frac{t_m-t_{0,m}}{T_B}\right), \end{aligned} \tag{7}$$

where $t_{0,m}$ represents the location of the target in the slow-time dimension, that is, the slow-time location of the target when the target is aligned with the normal axis of the antenna, and T_B represents the duration of the target echo in the slow-time dimension ($T_B = \theta_{3\,\mathrm{dB}}/\Omega_A$, where $\theta_{3\,\mathrm{dB}}$ represents the beam width of the antenna and Ω_A represents the rotational speed of the antenna).

Assume that the target is moving toward the radar in the radial direction at a uniform speed and its absolute velocity is v_0. Let the line-scan speed resulting from SSAR be denoted by v_A and the midpoint of the slow-time duration of the echo signal be used as the reference point. Thus, the slow-time instantaneous radial velocity of the target at the reference point for the SSAR system is $v_{r,M} = v_0 + (1/2)v_A\Omega_A T_B$. According to the SSAR theory, the corresponding slow-time instantaneous range of the target is

$$R(t_m) = R_0 - v_{r,M}(t_m - t_{0,m}) - \frac{1}{2}v_A\Omega_A(t_m - t_{0,m})^2, \tag{8}$$

where R_0 represents the reference distance, that is, the slant range of the target at the slow-time instant $t_{0,m}$.

According to the stationary phase principle, the Fourier transform corresponding to $p(t) = \operatorname{rect}(t/T_P)\exp(j\pi\mu t^2)$ is $p(f) = \operatorname{rect}(f/\mu T_p)\exp(-j\pi(f^2/\mu))$.

Performing a Fourier transform on (7) with respect to fast-time (t), we can obtain

$$\begin{aligned} S_{r,h}(f,t_m) &= p(f)\exp\left[-j2\pi f\frac{2R(t_m)}{C}\right] \\ &\cdot\exp\left[-j2\pi f_0\frac{2R(t_m)}{C}\right]\operatorname{rect}\left(\frac{t_m-t_{0,m}}{T_B}\right). \end{aligned} \tag{9}$$

Applying matched filtering and substituting $p(f)$ into (9), we can obtain

$$\begin{aligned} S^M{}_{r,h}(f,t_m) &= \operatorname{rect}\left(\frac{f}{\mu T_p}\right)\exp\left[-j2\pi f\frac{2R(t_m)}{C}\right] \\ &\cdot\operatorname{rect}\left(\frac{t_m-t_{0,m}}{T_B}\right)\exp\left[-j2\pi f_0\frac{2R(t_m)}{C}\right]. \end{aligned} \tag{10}$$

Performing an inverse Fourier transform (IFT) on $S^M{}_{r,h}(f, t_m)$, we can obtain

$$\begin{aligned} S^M{}_{r,h}(t,t_m) &= \mu T_p \sin c\left[\mu T_p\pi\left(t-\frac{2R(t_m)}{C}\right)\right] \\ &\cdot\operatorname{rect}\left(\frac{t_m-t_{0,m}}{T_B}\right)\exp\left[-j2\pi f_0\frac{2R(t_m)}{C}\right]. \end{aligned} \tag{11}$$

The expression for $S^M{}_{r,h}(t, t_m)$ is also the result generated after using a matched filter.

Performing a Fourier transform with respect to fast-time (t) on $S^M{}_{r,h}(t, t_m)$ again, we can obtain

$$\begin{aligned} S^M{}_{r,h}(f,t_m) &= \operatorname{rect}\left(\frac{f}{\mu T_p}\right)\exp\left[-j2\pi f\frac{2R(t_m)}{C}\right] \\ &\cdot\operatorname{rect}\left(\frac{t_m-t_{0,m}}{T_B}\right)\exp\left[-j2\pi f_0\frac{2R(t_m)}{C}\right] \\ &= \operatorname{rect}\left(\frac{f}{\mu T_p}\right)\operatorname{rect}\left(\frac{t_m-t_{0,m}}{T_B}\right) \\ &\cdot\exp\left[-j2\pi(f+f_0)\frac{2R(t_m)}{C}\right]. \end{aligned} \tag{12}$$

Substituting (8) into (12), we can obtain

$$\begin{aligned} S^M{}_{r,h}(f,t_m) &= \operatorname{rect}\left(\frac{f}{\mu T_p}\right)\operatorname{rect}\left(\frac{t_m-t_{0,m}}{T_B}\right) \\ &\cdot\exp\left\{-j2\pi(f+f_0)\frac{2}{C}\left[R_0 - v_{r,M}(t_m-t_{0,m})\right.\right. \\ &\left.\left.-\frac{1}{2}v_A\Omega_A(t_m-t_{0,m})^2\right]\right\}. \end{aligned} \tag{13}$$

Substituting $v_{r,M} = v_0 + (1/2)v_A\Omega_A T_B$ into (13), we can obtain

$$\begin{aligned} S^M{}_{r,h}(f,t_m) &= \mathrm{rect}\left(\frac{f}{\mu T_p}\right)\mathrm{rect}\left(\frac{t_m - t_{0,m}}{T_B}\right) \\ &\cdot \exp\left[-j2\pi(f+f_0)\frac{2}{C}R_0\right] \times \exp\left[j2\pi(f+f_0)\frac{2}{C}\right. \\ &\left.\cdot v_{r,M}(t_m - t_{0,m})\right] \\ &\cdot \exp\left\{j2\pi(f+f_0)\frac{2}{C}\left[\frac{1}{2}v_A\Omega_A(t_m - t_{0,m})^2\right]\right\} \\ &= \mathrm{rect}\left(\frac{f}{\mu T_p}\right)\mathrm{rect}\left(\frac{t_m - t_{0,m}}{T_B}\right) \\ &\cdot \exp\left[-j2\pi(f+f_0)\frac{2}{C}R_0\right] \times \exp\left[j2\pi(f+f_0)\right. \\ &\left.\cdot \frac{2}{C}\left(v_0 + \frac{1}{2}v_A\Omega_A T_B\right)(t_m - t_{0,m})\right] \\ &\cdot \exp\left\{j2\pi(f+f_0)\frac{2}{C}\left[\frac{1}{2}v_A\Omega_A(t_m - t_{0,m})^2\right]\right\}. \end{aligned} \tag{14}$$

Because $\exp[-j2\pi(f+f_0)(2/C)(1/2)v_A\Omega_A T_B t_m] = \exp[-j\pi(f+f_0)(2/C)v_A\Omega_A T_B t_m]$, we have

$$\begin{aligned} S'^M_{r,h}(f,t_m) &= S^M{}_{r,h}(f,t_m)\exp\left[-j\pi(f+f_0)\frac{2}{C}\right. \\ &\left.\cdot v_A\Omega_A T_B t_m\right] = \mathrm{rect}\left(\frac{f}{\mu T_p}\right)\mathrm{rect}\left(\frac{t_m - t_{0,m}}{T_B}\right) \\ &\cdot \exp\left[-j2\pi(f+f_0)\left(\frac{2}{C}R_0 + \frac{1}{C}v_A\Omega_A T_B t_{0,m}\right)\right] \\ &\times \exp\left\{j2\pi(f+f_0)\right. \\ &\left.\cdot \frac{2}{C}\left[v_0(t_m - t_{0,m}) + \frac{1}{2}v_A\Omega_A(t_m - t_{0,m})^2\right]\right\} \\ &= \mathrm{rect}\left(\frac{f}{\mu T_p}\right)\exp\left[-j2\pi(f+f_0)\right. \\ &\left.\cdot\left(\frac{2}{C}R_0 + \frac{1}{C}v_A\Omega_A T_B t_{0,m}\right)\right] \times \left\{\mathrm{rect}\left(\frac{t_m}{T_B}\right)\right. \\ &\left.\cdot \exp\left[j2\pi(f+f_0)\frac{2}{C}\left(v_0 t_m + \frac{1}{2}v_A\Omega_A {t_m}^2\right)\right]\right. \\ &\left.\otimes \delta(t_m - t_{0,m})\right\} = \mathrm{rect}\left(\frac{f}{\mu T_p}\right)\exp\left[-j2\pi(f+f_0)\right. \\ &\left.\cdot\left(\frac{2}{C}R_0 + \frac{1}{C}v_A\Omega_A T_B t_{0,m}\right)\right]F(t_m), \end{aligned} \tag{15}$$

where $F(t_m) = \mathrm{rect}(t_m/T_B)\exp[j2\pi(f+f_0)(2/C)(v_0 t_m + (1/2)v_A\Omega_A {t_m}^2)] \otimes \delta(t_m - t_{0,m})$.

Performing a Fourier transform with respect to slow-time (t_m) on $F(t_m)$, we can obtain

$$\begin{aligned} F(t_m) &\overset{f_m}{\longleftrightarrow} F(f_m) \\ &= \left\{\mathrm{rect}\left(\frac{f_m}{(f+f_0)(2/C)v_A\Omega_A T_B}\right)\right. \\ &\left.\cdot \exp\left[-j\pi\frac{f_m^2}{(f+f_0)(2/C)v_A\Omega_A}\right]\right. \\ &\left.\otimes \delta\left(f_m - (f+f_0)\frac{2}{C}v_0\right)\right\}\exp(-j2\pi t_{0,m}f_m). \end{aligned} \tag{16}$$

Performing a Fourier transform on $S'^M_{r,h}(f,t_m)$ with respect to slow-time (t_m) and substituting the result into $F(f_m)$, we can obtain

$$\begin{aligned} S'^M_{r,h}(f,f_m) &= \mathrm{rect}\left(\frac{f}{\mu T_p}\right) \\ &\cdot \exp\left[-j2\pi f\left(\frac{2}{C}R_0 + \frac{1}{C}v_A\Omega_A T_B t_{0,m} + \frac{v_0^2}{Cv_A\Omega_A}\right)\right] \\ &\cdot \exp\left[-j2\pi f_0\left(\frac{2}{C}R_0 + \frac{1}{C}v_A\Omega_A T_B t_{0,m} + \frac{v_0^2}{Cv_A\Omega_A}\right)\right] \\ &\times \mathrm{rect}\left(\frac{f_m - (f+f_0)(2/C)v_0}{(f+f_0)(2/C)v_A\Omega_A T_B}\right) \\ &\cdot \exp\left[-j\pi\frac{f_m^2}{(f+f_0)(2/C)v_A\Omega_A}\right] \\ &\cdot \exp\left(j2\pi\frac{v_0}{v_A\Omega_A}f_m\right)\exp(-j2\pi t_{0,m}f_m). \end{aligned} \tag{17}$$

Compensating (17) by $\exp[j\pi f_m^2/((f+f_0)(2/C)v_A\Omega_A)]$, we can obtain

$$\begin{aligned} S''^M_{r,h}(f,f_m) &= S'^M_{r,h}(f,f_m)\exp\left[j\pi\right. \\ &\left.\cdot\frac{f_m^2}{(f+f_0)(2/C)v_A\Omega_A}\right] = \mathrm{rect}\left(\frac{f}{\mu T_p}\right) \\ &\cdot \exp\left[-j2\pi f\left(\frac{2}{C}R_0 + \frac{1}{C}v_A\Omega_A T_B t_{0,m}\right.\right. \\ &\left.\left. + \frac{v_0^2}{Cv_A\Omega_A}\right)\right] \times \exp\left[-j2\pi f_0\left(\frac{2}{C}R_0\right.\right. \\ &\left.\left. + \frac{1}{C}v_A\Omega_A T_B t_{0,m} + \frac{v_0^2}{Cv_A\Omega_A}\right)\right] \\ &\times \mathrm{rect}\left(\frac{f_m - (f+f_0)(2/C)v_0}{(f+f_0)(2/C)v_A\Omega_A T_B}\right)\exp\left(j2\pi\frac{v_0}{v_A\Omega_A}\right. \\ &\left.\cdot f_m\right)\exp(-j2\pi t_{0,m}f_m). \end{aligned} \tag{18}$$

In (18), the term $\mathrm{rect}((f_m-(f+f_0)(2/C)v_0)/((f+f_0)(2/C)v_A\Omega_A T_B))$, which is denoted by $(*)$, affects the final compression.

Clearly, the $(*)$ term is related to the velocity of the target, the bandwidth of the transmitting signal, the line-scan speed of the system, and the beam width. The line-scan speed and the beam width each have a positive effect on the final compression, that is, increasing the line-scan speed of the system and the beam width can improve the compression. Increasing the line-scan speed is limited by the antenna size, and the beam width has an upper limit of approximately 38° according to the SSAR theory. Thus, the improving space of the line-scan speed is larger than that of the beam width. The velocity of the target and the bandwidth of the transmitting signal have a negative effect on the final compression (under the same condition as the $\Delta \ll 1$ condition described in the following sections). For different fast-time frequencies, the slow-time frequencies are distributed in different centers (which are modulated by the velocity of the target) and different widths (which are modulated by the bandwidth of the transmitting signal). The more discrete the distribution centers are and the greater the variations in the distribution widths are, the greater their effect on the final compression is.

Here we define

$$\Delta = \sqrt{{\Delta_1}^2 + {\Delta_2}^2} = \frac{B}{f_0}\sqrt{1+\left(\frac{v_0}{v_A\theta_{3\,\mathrm{dB}}}\right)^2}, \tag{19}$$

where $\Delta_1 = B(2/C)v_0/f_0(2/C)v_A\Omega_A T_B = Bv_0/f_0 v_A\theta_{3\,\mathrm{dB}}$ and $\Delta_2 = B(2/C)v_A\Omega_A T_B/f_0(2/C)v_A\Omega_A T_B = B/f_0$.

When $\Delta \ll 1$, the $(*)$ term is expressed as follows:

$$\begin{aligned}&\mathrm{rect}\left(\frac{f_m-(f+f_0)(2/C)v_0}{(f+f_0)(2/C)v_A\Omega_A T_B}\right)\\ &\quad\approx \mathrm{rect}\left(\frac{f_m-f_0(2/C)v_0}{f_0(2/C)v_A\Omega_A T_B}\right).\end{aligned} \tag{20}$$

Thus, we can obtain

$$\begin{aligned}S_{r,h}^{\prime\prime M}(f,f_m) \approx{}& \mathrm{rect}\left(\frac{f}{\mu T_p}\right)\exp\left[-j2\pi f\left(\frac{2}{C}R_0\right.\right.\\ &\left.\left.+\frac{1}{C}v_A\Omega_A T_B t_{0,m}+\frac{v_0^2}{Cv_A\Omega_A}\right)\right]\\ &\times\exp\left[-j2\pi f_0\left(\frac{2}{C}R_0+\frac{1}{C}v_A\Omega_A T_B t_{0,m}\right.\right.\\ &\left.\left.+\frac{v_0^2}{Cv_A\Omega_A}\right)\right]\times\mathrm{rect}\left(\frac{f_m-f_0(2/C)v_0}{f_0(2/C)v_A\Omega_A T_B}\right)\exp\left(j2\pi\right.\\ &\left.\cdot\frac{v_0}{v_A\Omega_A}f_m\right)\exp\left(-j2\pi t_{0,m}f_m\right).\end{aligned} \tag{21}$$

Performing an IFT on (21) with respect to slow-time and fast-time, we can obtain

$$\begin{aligned}S_{r,h}^{\prime\prime M}(f,f_m) \overset{t\blacklozenge t_m}{\longleftrightarrow} S_{r,h}^{\prime\prime M}(t,t_m) ={}& \left(\mu T_p\right)\sin c\left[\mu T_p\pi\left(t\right.\right.\\ &\left.\left.-\left(\frac{2}{C}R_0+\frac{1}{C}v_A\Omega_A T_B t_{0,m}+\frac{v_0^2}{Cv_A\Omega_A}\right)\right)\right]\times\left(\frac{2}{\lambda}\right.\\ &\left.\cdot v_A\Omega_A T_B\right)\sin c\left[\frac{2}{\lambda}v_A\Omega_A T_B\pi\left(t_m\right.\right.\\ &\left.\left.-\left(t_{0,m}-\frac{v_0}{v_A\Omega_A}\right)\right)\right]\times\exp\left(j2\pi\frac{2}{\lambda}v_0 t_m\right)\\ &\cdot\exp\left[-j2\pi f_0\left(\frac{2}{C}R_0+\frac{1}{C}v_A\Omega_A T_B t_{0,m}+\frac{v_0^2}{Cv_A\Omega_A}\right)\right].\end{aligned} \tag{22}$$

In the final compression, the amplitude of the echo signal improves $(\mu T_p)*((2/\lambda)v_A\Omega_A T_B)$ times, where $\mu T_p = B_t$ is the bandwidth of the transmitting signal and $(2/\lambda)v_A\Omega_A T_B = B_{t_m}$ is the bandwidth of the LFM signal formed by the line-scan in the azimuth dimension. Thus, the capability of the radar system to detect dim targets is significantly improved.

From (22), the location of the target obtained following compression is $(2/C)R_0 + (1/C)v_A\Omega_A T_B t_{0,m} + v_0^2/Cv_A\Omega_A$ in the fast-time dimension, which gives the range, and $t_{0,m} - v_0/v_A\Omega_A$ in the slow-time dimension, which gives the azimuth. However, the actual location is $((2/C)R_0\ \ t_{0,m})$, indicating that there is a large difference, especially in the azimuth dimension, and this difference is caused by the velocity of the target.

From (22), we can obtain

$$\begin{aligned}\frac{2}{C}R_0+\frac{1}{C}v_A\Omega_A T_B t_{0,m}+\frac{v_0^2}{Cv_A\Omega_A}&=\lambda_1,\\ t_{0,m}-\frac{v_0}{v_A\Omega_A}&=\lambda_2.\end{aligned} \tag{23}$$

In (23), there are three unknown variables but only two equations. Therefore, the precise location of the target cannot be determined. Another equation that contains the three unknown variables is required to determine the location of the target. The difference in the line-scan speed provides two additional equations, so that we can obtain

$$\begin{aligned}\frac{2}{C}R_0+\frac{1}{C}v_A\Omega_A T_B t_{0,m}+\frac{v_0^2}{Cv_A\Omega_A}&=\lambda_1,\\ t_{0,m}-\frac{v_0}{v_A\Omega_A}&=\lambda_2,\\ \frac{2}{C}R_0+\frac{1}{C}v_A'\Omega_A T_B t_{0,m}+\frac{v_0^2}{Cv_A'\Omega_A}&=\lambda_3,\\ t_{0,m}-\frac{v_0}{v_A'\Omega_A}&=\lambda_4.\end{aligned} \tag{24}$$

These four equations contain the three unknown variables. Solving (24) for the unknowns, we can obtain

$$\begin{aligned} v_0 &= \frac{(\lambda_2 - \lambda_4)\,\Omega_A}{(v_A - v_A')/v_A v_A'} = \frac{(\lambda_2 - \lambda_4)\,\Omega_A v_A v_A'}{v_A - v_A'}, \\ t_{0,m} &= \lambda_2 + \frac{v_0}{v_A \Omega_A}, \\ R_0 &= \frac{C}{2}\left(\lambda_1 - \frac{1}{C} v_A \Omega_A T_B t_{0,m} - \frac{v_0^2}{C v_A \Omega_A}\right) \\ &= \frac{C}{2}\lambda_1 - \frac{1}{2} v_A \Omega_A T_B t_{0,m} - \frac{1}{2}\frac{v_0^2}{v_A \Omega_A}. \end{aligned} \tag{25}$$

It is recommended that two slow-time dimension equations be used. First, the velocity of the target can be determined. Then, the location of the target in the slow-time dimension is determined. The range of the target can be determined using the equation with a relatively high line-scan speed. If the difference between the two line-scan speeds is excessively high, the target detection will be affected. To improve the solution accuracy, it is recommended that the fast-time dimension equation with a relatively high line-scan speed be used to determine the range of the target. Simulations showed that this algorithm has greater accuracy when the velocity of the target is within a certain range. The performance of this algorithm decreases when the velocity of the target is very high. To address this issue, the velocity range of the target is divided into intervals, and the interval in which the velocity of the target is the lowest is selected as the basic interval for processing. When searching in other intervals, phase compensation is performed with the maximum velocity in the basic interval as the baseline value (the velocity in the middle of the other interval is $2n$ times the maximum velocity in the basic interval). The detection results obtained from all of the intervals are integrated (because of the difference in the line-scan speed) based on the minimum distance criterion.

By summing up the above algorithm, the SSAR signal processing procedure is summarized in Figure 1.

4. Computer Simulation Experiment and Analysis

Computer simulations are performed, and the SSAR algorithm is used to obtain the spatial distribution of the energy of the targets, based on which the parameters of the targets (the azimuth, the range, and the velocity) are determined. The simulation results are compared with the true values of the target parameters to evaluate the performance of the algorithm. In addition, the results of SNR improvement are analyzed. The whole simulation process is an intermediate-frequency digital simulation that is performed in MATLAB.

Table 1 lists the parameters of the radar system and the targets used for the simulations. Window functions can be used to reduce the effect of the range and angle side-lobes on the processing results. Common window functions include the Hanning window, the Hamming window, and the Kaiser window. In the present study, the Kaiser window function is used for weighting [17] (time-domain weighting is used for the range dimension, and frequency-domain weighting is used for the azimuth dimension). The value of the Kaiser window parameter (β) is 2.5 in the simulations.

4.1. Simulation 1: The Range-Azimuth Energy Distribution of the Targets at Different Line-Scan Range. Figure 2 shows the range-azimuth energy distribution at a line-scan range of 1.8 (relative to the half-wavelength) obtained after processing the radar data generated by the simulations.

Figure 2(a) shows the energy distribution before detecting with the noise gate. To accentuate the effect of the accumulation of the signal energy of the targets in the noise, the amplitude of the processed signal is normalized and expressed in dB. To simplify the presentation, all of the values below −15 dB are shown as −15 dB. Figure 2(b) shows the energy distribution after detecting with the noise gate. To accentuate the effect of the accumulation of the signal energy of the targets, the amplitude of the signal is not expressed in dB.

Figure 3 shows the range-azimuth energy distribution at a line-scan range of 1.5 (relative to the half-wavelength).

Figure 3(a) shows the energy distribution before detecting with the noise gate, with the settings equal to those used for the case in Figure 2(a). Figure 3(b) shows the energy distribution after detecting with the noise gate, with the settings equal those used for the case in Figure 2(b). In Figures 2 and 3, the azimuth interval is the angle of the antenna rotation within a PRI, and the range interval is the range corresponding to the sampling time. All the values are obtained by digitizing the signals.

4.2. Simulation 2: The Parameters (Range, Azimuth, and Velocity) of the Targets. Figures 2 and 3 show the energy of the targets accumulated in the range and azimuth dimensions rather than the actual location of the targets. From the locations of the targets shown in Figures 2(b) and 3(b), the difference in the line-scan speed for line-scan ranges of 1.8 and 1.5 (relative to the half-wavelength) is insignificant, and therefore, the set of equations shown in (24) can be established by pairing according to the minimum range principle. By solving this set of equations, the values of the target parameters (range, azimuth, and velocity) can be determined. Table 2 lists the values of the target parameters obtained from the simulations using the parameters listed in Table 1 (azimuth unit: deg.; range unit: km; velocity unit: m/s).

Table 2 shows that the simulation results are very close to the true values, which demonstrates that this algorithm is effective and can meet the requirements of the warning radar.

It is important to note that the difference between the two line-scan ranges has practical upper and lower limits. Smaller differences between the two line-scan ranges result in larger errors in the solution, and larger differences between the two line-scan ranges may result in the targets not being detected within the shorter line-scan range. In either case, the third independent equation cannot be established.

4.3. Simulation 3: Simulation and Analysis of SNR Improvement. Generally, the traditional signal processing methods of

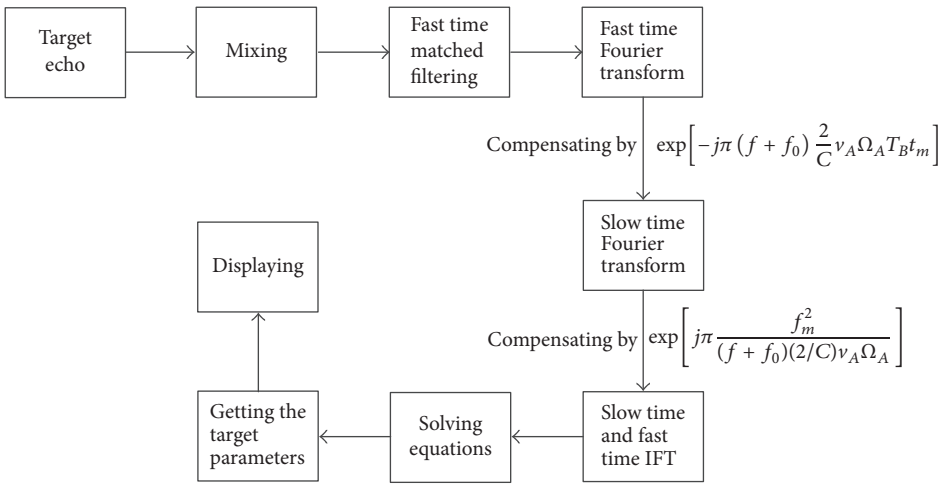

Figure 1: SSAR signal processing procedure.

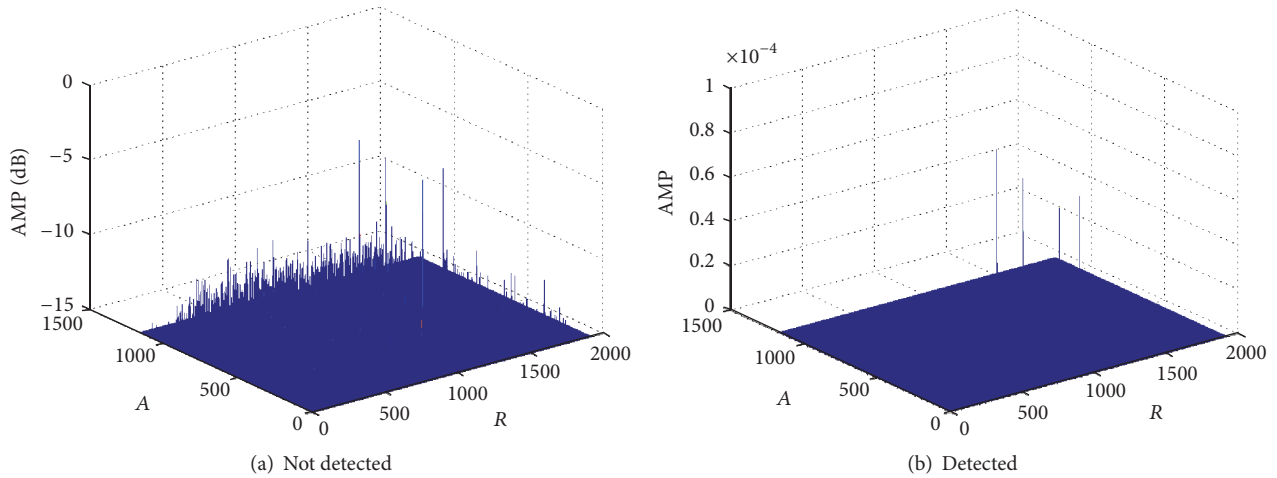

(a) Not detected (b) Detected

Figure 2: Range-azimuth-amplitude distribution at a line-scan range of 1.8.

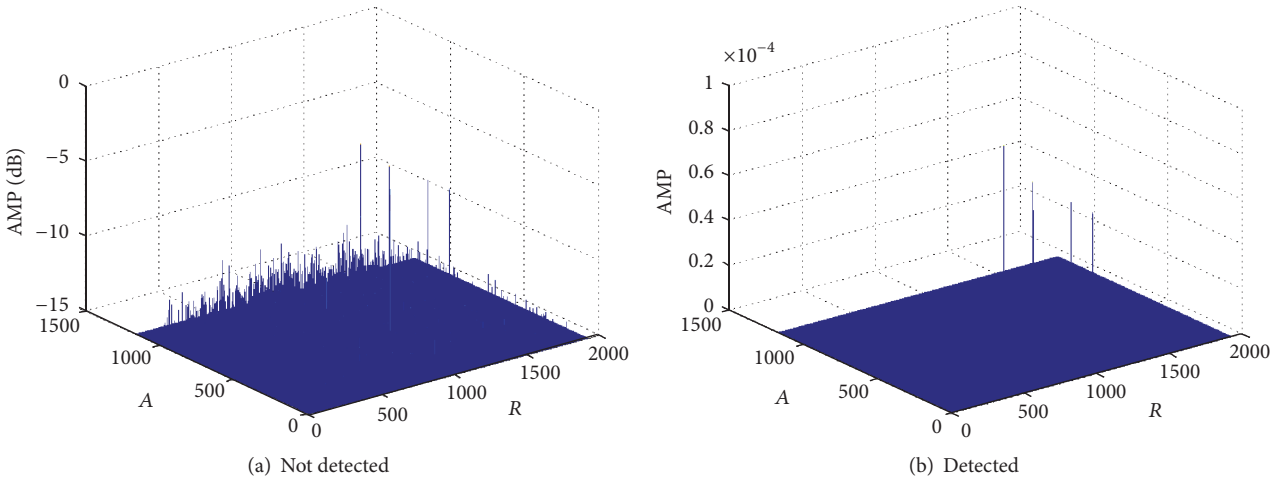

(a) Not detected (b) Detected

Figure 3: Range-azimuth-amplitude distribution at a line-scan range of 1.5.

Table 1: Parameter values for SSAR signal processing simulations.

Radar parameters	
Carrier frequency (f_0)	300 MHz
PRI	1,000 μs
Pulse width (τ)	100 μs
Bandwidth (B)	10 MHz
Rotational speed of the sector-scan antenna (Ω_a)	36°/s
3 dB beam width	30°
Transmitting signal power (P_t)	10 kW
Transmitting antenna gain (G_t)	30 dB
Receiving antenna gain (G_r)	30 dB
Initial angle of the antenna rotation	0°
Line-scan range of the antenna	[1.8, 1.5] ∗ wavelength/2
Line-scan cycle of the antenna	PRI
Target parameters (true values)	
Number	4
Slant range	[98, 100, 103, 105] km
Azimuth	[18, 20.5, 22, 24]°
Velocity	[100, 150, 180, 200] m/s
Target heading angle (relative to the radial direction)	[0, 0, 0, 0]°
RCS	[0.1, 0.1, 0.1, 0.1] m^2
Simulation parameters	
SNR (receiving point)	−33 dB
Range window	[0.6, 0.76] ∗ PRI ∗C/2 km
Azimuth window	[0, 42]°
Signal format	LFM in the exponential form
Sampling rate (range dimension)	1.2B (analytic signals)

Notes. The noise is assumed to be Gaussian white noise; transmission losses are not considered but can be included in the SNR; and the false-alarm probability (P_f) is set to 10^{-6} for range detection. 1.2B: 1.2 times bandwidth (B).

Table 2: Simulation results for SSAR and true values of the targets.

Target number	Simulation results			True values		
	Range	Azimuth	Velocity	Range	Azimuth	Velocity
(1)	98.024	17.964	98.960	98	18	100
(2)	100.021	20.520	149.854	100	20.5	150
(3)	103.014	22.104	180.956	103	22	180
(4)	105.021	23.904	197.920	105	24	200

ground-based sector-scan radar only do signal compression in fast-time dimension (i.e., range dimension). Supposing that the farthest target input SNR is −20 dB, the rest of the simulation parameters are shown in Table 1. Figure 4 shows the range-amplitude distribution of the targets after signal processing by the traditional methods. SSAR does signal compression in both fast-time dimension and slow-time dimension (i.e., azimuth dimension). Supposing that the farthest target input SNR is −33 dB and the line-scan range is 1.8 (relative to the half-wavelength), the rest of the simulation parameters are also shown in Table 1. Figure 5 shows the range-amplitude distribution of the targets after signal processing by the algorithm proposed in this paper.

It can be seen from Figure 4 that the amplitude of the farthest target is about −1.2 dB (using −20 log 10( ) mode to calculate, the same below), and the noise is almost below −3.6 dB. Therefore, after signal processing, SNR is 2.4 dB. Considering that the input SNR is −20 dB, the signal processing gain of the traditional methods is about 22.4 dB.

It can be seen from Figure 5 that the amplitude of the farthest target is about −2.5 dB, and the noise is almost below −10.5 dB. Therefore, after signal processing, SNR is 8 dB. Considering that the input SNR is −33 dB, the total signal processing gain is about 41 dB with two parts of contribution. 22.4 dB in 41 dB is obtained by the traditional signal compression in fast-time dimension, and 18.6 dB in 41 dB is obtained by the signal compression in slow-time dimension, that is, obtained by line-scan mode.

Compared with the traditional signal processing methods, the proposed signal processing algorithm improves the

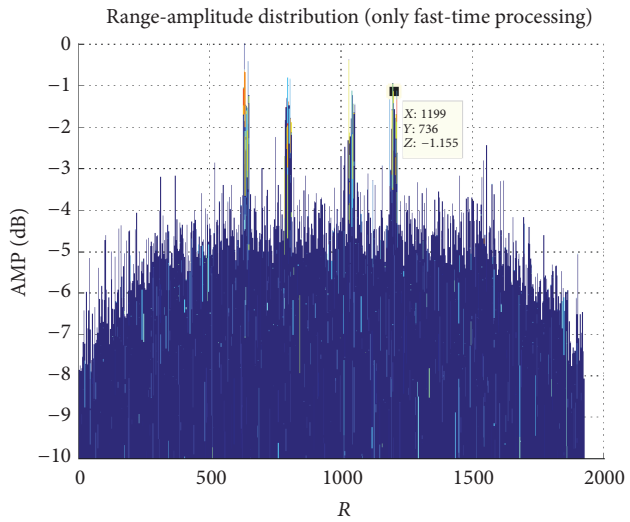

Figure 4: Range-amplitude distribution of the targets (by the traditional signal processing methods).

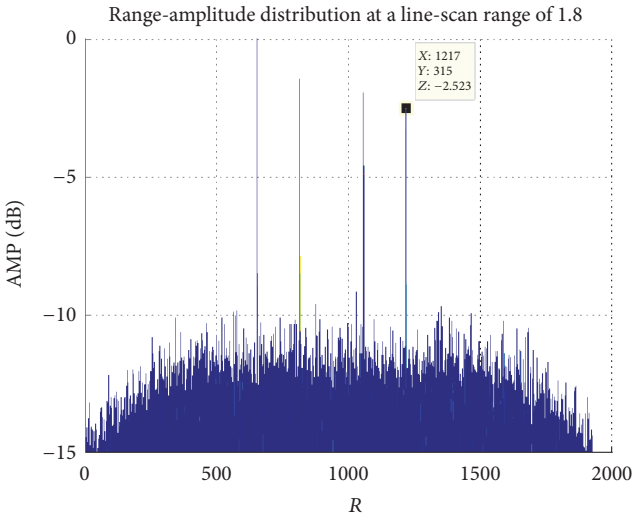

Figure 5: Range-amplitude distribution of the targets (by the proposed signal processing algorithm).

SNR by about 18.6 dB. Therefore, the algorithm can improve the detection performance of dim targets.

5. Conclusions

In the present study, an SSAR echo signal model is developed based on the "stop-go" model. Next, using the 2D matched filtering approach, an SSAR signal processing algorithm is proposed and deduced in detail. The performance of the algorithm is then verified through simulations. The simulation results show that the SSAR signal processing algorithm concentrates the signal energy of the targets and increases the SNR, thereby demonstrating that SSAR can detect dim targets with high accuracy. In addition, the proposed algorithm processes all the data of the radar scanning space. This algorithm requires a relatively short computation time. Furthermore, the majority of the complex computations can be performed by the FFT algorithm, so the computing speed is high.

Conflicts of Interest

The authors declare that they have no conflicts of interest.

References

[1] W. Wang and Z. Wang, "Top down plan on anti-stealth techniques of fixed early warning radar," *Journal of Northwestern Polytechnical University*, vol. 32, no. 6, pp. 956–961, 2014.

[2] L. Ding, F. Geng, and J. Chen, *Radar Principles*, Publishing House of Electronics Industry, Beijing, China, 4th edition.

[3] J. Wang and X. Liu, "Automatic correction of range migration in SAR imaging," *IEEE Geoscience and Remote Sensing Letters*, vol. 7, no. 2, pp. 256–260, 2010.

[4] L. I. Xi, G. Liu, and J. Ni, "Autofocusing of ISAR images based on entropy minimization," *IEEE Transactions on Aerospace and Electronic Systems*, vol. 35, no. 4, pp. 1240–1252, 1999.

[5] R. Sharif and S. S. Abeysekera, "Efficient wideband signal parameter estimation using a radon-ambiguity transform slice," *IEEE Transactions on Aerospace and Electronic Systems*, vol. 43, no. 2, pp. 673–688, 2007.

[6] W.-C. Chen, Z. Bao, and M.-D. Xing, "Keystone transformation based ISAR imaging at the low SNR level," *Journal of Xidian University*, vol. 30, no. 2, pp. 155–159, 2003.

[7] H. Li, Y. Zhang, and X. L. He, "The modification of ISAR envelope correlation algorithm," *Journal of Microwaves*, vol. 22, no. 6, pp. 147–151, 2006.

[8] Y. Huang, Y. Zheng, and Z. Bao, "The SAR/ISAR autofocus based on the multiple dominant scatterers synthesis," *Journal of Xidian University (Natural Science)*, vol. 28, no. 1, pp. 105–109, 2001.

[9] Y. Li, M. Xing, J. Su, Y. Quan, and Z. Bao, "A new algorithm of isar imaging for maneuvering targets with low SNR," *IEEE Transactions on Aerospace and Electronic Systems*, vol. 49, no. 1, pp. 543–557, 2013.

[10] X. Z. Tian, S. S. Zhang, and L. N. Pang, "Range cell migration correction for dim maneuvering target detection," in *Proceedings of the IEEE Radar Conference*, pp. 1247–1250, IEEE, Ohio, Ohio, USA, May 2014.

[11] C. Dai and X. Zhang, "Range cell migration correction for bistatic SAR image formation," in *Proceedings of the 32nd IEEE International Geoscience and Remote Sensing Symposium, IGARSS '12*, pp. 404–407, July 2012.

[12] S. Li, H. Sun, B. Zhu, and R. Liu, "Two-dimensional NUFFT-based algorithm for fast near-field imaging," *IEEE Antennas and Wireless Propagation Letters*, vol. 9, pp. 814–817, 2010.

[13] S.-Y. Wu, G.-S. Liao, S.-Q. Zhu, and Z.-W. Yang, "A new method for radar maneuvering target detection based on matched filtering in two-dimensional frequency domain," *Acta Electronica Sinica*, vol. 40, no. 12, pp. 2415–2420, 2012.

[14] S. Zhu, G. Liao, D. Yang, and H. Tao, "A new method for radar high-speed maneuvering weak target detection and imaging," *IEEE Geoscience and Remote Sensing Letters*, vol. 11, no. 7, pp. 1175–1179, 2014.

[15] S. Zhu, G. Liao, Y. Qu, Z. Zhou, and X. Liu, "Ground moving targets imaging algorithm for synthetic aperture radar," *IEEE*

Transactions on Geoscience and Remote Sensing, vol. 49, no. 1, pp. 462–477, 2011.

[16] H. Zhang, *ISAR imaging of high speed moving targets [Ph.D thesis]*, Xidian University, Xi'an, China, 2007.

[17] I. G. Cumming and F. H. Wong, *Digital processing of synthetic aperture radar data: algorithms and implementation [M.S. thesis]*, Publishing House of Electronics Industry, Beijing, China, 2012.